**Atmospheric
Chemistry
and Physics
Discussions**

Closure on the single scattering albedo in the WRF-Chem framework using data from the MILAGRO campaign

J. C. Barnard[1], J. D. Fast[1], G. Paredes-Miranda[2], and W. P. Arnott[2]

[1]Pacific Northwest National Laboratory, Richland, Washington, USA
[2]University of Nevada, Reno, Nevada, USA

Correspondence to: J. C. Barnard (james.barnard@pnl.gov)

ACPD

9, 5009–5054, 2009

Closure on the single scattering albedo

J. C. Barnard et al.

Title Page

Abstract	Introduction
Conclusions	References
Tables	Figures

| ◄◄ | ►► |
| ◄ | ► |

| Back | Close |

Full Screen / Esc

Printer-friendly Version

Interactive Discussion

Closure on the single scattering albedo

J. C. Barnard et al.

Abstract

Data from the MILAGRO field campaign, which took place in the Mexico City Metropolitan Area (MCMA) during March 2006, is used to perform a closure experiment between aerosol chemical properties and aerosol optical properties. Measured aerosol chemical properties, obtained from the MILAGRO T1 site, are fed to two different "chemical to optical properties" modules. One module uses a sectional approach and is identical to that used in the WRF-Chem model, while the other is based on a modal approach. This modal code is employed as an independent check on the WRF-Chem module. Both modules compute aerosol optical properties and, in particular, the single-scattering albedo, ϖ_0, as a function of time. The single-scattering albedos are compared to independent measurements obtained from a photoacoustic spectrometer (PAS). Because chemical measurements of the aerosol coarse mode were not available, and the inlet of the PAS could not ingest aerosols larger than about 2 to 3 μm, we focus here on the fine-mode ϖ_0. At 870 nm, the wavelength of the PAS measurements, the agreement between the computed (modal and WRF-Chem) and observed fine-mode ϖ_0, averaged over the course of the campaign, is reasonably good. The observed ϖ_0 value is 0.77, while for both modules, the calculated value was 0.75 resulting in a difference of 0.02 between observations and both computational approaches. This difference is less than the uncertainty of the observed ϖ_0 values (6%, or 0.05), and therefore "closure" is achieved, at least for mean values. After adjusting some properties of black carbon absorption and mass concentration within plausible uncertainty limits, the two modules simulate well the diurnal variation of ϖ_0, and the absorption coefficient, B_{abs}, but are less successful in calculating the variation of the scattering coefficient, B_{scat}. This difficulty is probably caused by the presence of larger particles during the day when windblown dust is ubiquitous; this dust likely increases the proportion of large particles introduced into the PAS. The dust also contributes to a very large aerosol mass loading in the coarse mode, and neglect of the coarse mode may cause significant errors, estimated to be as large as 0.07, in the calculation and measurement

of ambient ϖ_0. Finally, the observed ϖ_0 is compared to the ϖ_0 computed by the full WRF-Chem model, which includes prognostic aerosol chemistry. Unlike the results discussed above, a comparison between observed and simulated ϖ_0 values reveals major differences. This large discrepancy is probably due, in part, to poor characterization of emissions near the T1 site, particularly black carbon emissions.

1 Introduction

1.1 Motivation and goals

Radiative aerosol forcing of climate is a topic under active study with important implications for climate predictions. These predictions are often provided by global climate models, which in turn rely on parameterizations of the myriad complex physical processes of the climate system. The path to developing and implementing these parameterizations and associated code modules is long and complex. An important step along this path is the testing of aerosol modules, prior to implementation in global climate models. As noted by Ghan and Schwartz (2007), regional models provide an important test bed for evaluating these modules by comparing regional model simulations, which contain these modules, with field data.

The WRF-Chem model (Fast et al., 2006; Grell et al., 2005) represents a well-known example of a regional model being used as a test bed for aerosol (and other) modules (Fast et al., 2009). This model includes a scheme to calculate aerosol optical properties from aerosol chemical properties, and here we examine the ability of this module to predict aerosol single scattering albedo, ϖ_0. This examination is done by comparing WRF-Chem simulations of ϖ_0 to field measurements of the same, obtained as part of the MILAGRO field campaign that took place in March 2006 in the Mexico City Metropolitan Area (MCMA).

The comparison of observed and aerosol optical properties will be explored through the use of a "closure" experiment, as defined by Quinn and Coffman (1998). In these

experiments an aerosol property is measured, for example, ϖ_0, and then compared with calculations from a model. The model receives as input chemical and aerosol size distribution information that is completely independent of the measurements used to derive ϖ_0. Closure is deemed successful if the calculated and measured aerosol
5   property agrees within experimental uncertainties. We note editorially that closure is much more meaningful if the uncertainties are small.

This closure study, illustrated schematically in Fig. 1, will attempt to achieve three goals. The first and most important goal is to evaluate the physical verisimilitude of the WRF-Chem aerosol chemical-to-optical module (CTOM). As noted by Ghan and
10 Schwartz (2007) and Quinn et al. (1996), closure experiments are a particularly good way to uncover model shortcomings, because differences between simulations and observations can be associated with specific processes, which once identified, can be improved. The second goal is a "physical" examination of ϖ_0 in which we ask: What physical processes explain the value and behavior of ϖ_0? Finally, as the third goal,
15 we insert the tested stand-alone CTOM back into the WRF-Chem model, and then run full WRF-Chem simulations to see how well the full-blown model, with its complex interplay of process-related modules (emissions, chemical reactions, transport, etc.) predicts ϖ_0. From this procedure we can propose improvements to the WRF-Chem model, or its input data, aimed at improving simulations of aerosol optical properties,
20 at least in the MCMA region.

1.2   Prior art

Closure experiments that examine the relationship between aerosol chemical and optical properties have a long history. Almost all these experiments follow the schema described above in which aerosol optical properties are measured and compared with
25 calculated values from a model. Some of these studies attempt closure on a small volume in the atmosphere, known as a local closure, while other experiments attempt closure on the entire atmospheric column (Russell and Heintzenberg, 2000). A landmark local closure study, with a particularly detailed characterization of closure uncer-

Title Page	
Abstract	Introduction
Conclusions	References
Tables	Figures
◄◄	►►
◄	►
Back	Close

Full Screen / Esc

Printer-friendly Version

Interactive Discussion

tainties, is described in Quinn and Coffman (1998). They used data from the Aerosol Characterization Experiment (ACE-1), assumed a simplified chemistry, and accounted for relative humidity effects. They found closure on scattering and backscatter coefficients within experimental uncertainties in the aerosol submicron size range. Closure was not achieved in the supermicron size range, ascribed in part to difficulties in measuring coarse mode aerosol properties.

Numerous other closure experiments have demonstrated that closure with reasonably small discrepancies between calculated and observed aerosol optical properties is achievable. For example, Wang et al. (2002) describe an exhaustive closure experiment that relies on aircraft data from the ACE-Asia field campaign. The closure variable was chosen to be aerosol extinction at 525 nm, which was inferred from optical depth measurements made by the airborne AATS-14 radiometer (Schmid et al., 2000). For various flight vertical profiles, calculated and measured extinctions are reasonably close, and the calculated profiles follow the considerable vertical variations in the measured profiles quite well. In dust layers, the closure was not as good, however, and this lack of agreement is probably caused by using spherical shapes to represent irregularly shaped dust particles when calculating extinction. This closure experiment can be considered as a local closure that extends through the atmospheric column.

Relatively recent aerosol closure or closure-like studies, similar in spirit to those described above, include Chaudhry et al. (2007), Cook et al. (2007), Sciare et al. (2005), Malm et al. (2005), Mallet et al. (2003), Fiebig et al. (2002), and Pesava et al. (2001). The work of Fiebig et al. (2002), Mallet et al. (2003), and Chaudhry et al. (2007) represent examples of full column closure, wherein aerosol chemical and size properties are measured at the surface and/or with aircraft, and are used to calculate columnar aerosol optical properties. Fiebig et al. (2002) use surface and aircraft measurements and find closure to within 25% between calculated columnar optical thickness, inferred from aircraft size distribution data and simplified chemistry, and columnar optical thickness measured by a ground-based sunphotometer. Mallet et al. (2003) used surface chemical and size distribution measurements to find ϖ_0 and asymmetry parameter,

Closure on the single scattering albedo

J. C. Barnard et al.

Printer-friendly Version

Interactive Discussion

g. They compare these aerosol properties with the same obtained from columnar AERONET sun photometer measurements, and the agreement is remarkably good, considering that ground-based inferences of the aerosol properties are compared with columnar measurements of these quantities. At 550 nm, the difference in the averages of AERONET ϖ_0 and calculated ϖ_0 was only 0.02.

2 Methodology

2.1 The T1 single-scattering albedo closure experiment

Our closure experiment builds on elements of these previous efforts, with several important advantages. The first of these is that the MILAGRO campaign provides one of the most comprehensive set of chemical measurements in existence, including organic carbon (OC), black carbon (BC)[1], and many inorganic species from the Particle-into-Liquid Sampler (PILS) instrument, as well as size segregated non-refractory species from the Aerodyne Mass Spectrometer. These instruments and their associated measurements will be discussed later. The MILAGRO chemical measurements represent one of the most comprehensive in existence. Second, complications from the hydroscopic growth of aerosols are minimized in the MCMA area because of the very low relative humidity. This considerably simplifies the study of the connection between aerosol chemical and optical properties, although we fully acknowledge that hydroscopic growth is an important part of understanding aerosol radiative forcing. We concentrate here on ϖ_0 as the optical property of interest. This parameter is critically important for radiative transfer calculations of direct aerosol forcing, and its magnitude can determine whether an aerosol heats or cools the atmosphere (Ramanathan et al.,

---

[1]We note here that some authors (e.g., Andreae and Gelencsér, 2006) prefer to distinguish between BC and elemental carbon, EC. For the purpose of this paper, we consider these quantities identical and use the terms BC and EC interchangeably.

2001; Heintzenberg et al., 1997). Single-scattering albedos obtained from various MI-LAGRO instruments have been described by Marley et al. (2009); however, we rely only on ϖ_0 inferences based on absorption measurements from a photoacoustic spectrometer (PAS) deployed at the MILAGRO T1 site during most of March 2006. The

⁵ location of this site, as well as the other major MILAGRO sites, is shown in Fig. 2. The latitude, longitude, and elevation of the site are 19.7031° N, 98.9820° W, and 2270 m, respectively.

2.2 Optical measurements

The PAS situated at site T1 is described in Arnott et al. (1999). This instrument uses
¹⁰ sound pressure produced by light absorption in an acoustic resonator to measure aerosol absorption. To find ϖ_0, scattering measurements are required, and these also are obtained from the PAS, using reciprocal nephelometry (Rahmah et al., 2006). The use of this particular combination of measurements to find ϖ_0 is described in Paredes-Miranda et al. (2008). At the T1 site, the PAS measurements were made at only one
¹⁵ wavelength, λ, of 870 nm. For this study, focusing on ϖ_0 at this wavelength is advantageous because we avoid the possibly major complications of dust (Sokolik and Toon, 1999) and organic carbon absorption, which may become significant at wavelengths less than about 600 nm (Barnard et al., 2008, and references therein); this important case is left to a future paper. We rely solely on PAS absorption measurements, be-
²⁰ cause these measurements are made without filter substrates. Recent evidence (Lack et al., 2008; Subramanian et al., 2007) suggests that filter-based measurements of absorption, made in the presence of large amounts of organic carbon, could be highly suspect because of soiling of the filter by the organic component of the aerosol.

Average absorption values were produced every two minutes, and these were aver-
²⁵ aged over half-hour intervals. The 30-min averaged values are used in this study. The uncertainty of the absorption measurements is 10%, while the uncertainty of the scattering measurements is 15%. These are estimates of systematic error (as opposed to random error) and are not reduced by averaging. Considering these values, the uncer-

tainty in the inferred values of ϖ_0 is about 6%. If the particles are large, the magnitude of the scattering measurements will always be less than the true scattering because of difficulties in measuring the forward scattering peak, which becomes significantly more prominent as the particle size increases. However, optical properties of very large par-
5 ticles, with aerodynamic diameters greater than 2 to 3 μm, were not measured by the PAS because of line and inlet losses that effectively "cut off" large particle sizes. Within this range, we assume that the largest particles that were measured did not exceed 2.5 μm in aerodynamic diameter, consistent with $PM_{2.5}$ measurements. (Within the range of 2 to 3 μm, our calculations show that the exact size chosen for the cut-off
10 diameter has little effect on the results.) Because of this cut-off in particle size, the ϖ_0 values discussed here should be considered as "fine mode" values. If there is a considerable aerosol mass in the coarse mode, it is possible that the fine mode value will not represent well the ambient ϖ_0 as discussed in Sect. 3.5.

2.3 Aerosol chemical measurements

15 Aerosol chemical measurements included elemental carbon (EC), aerosol organic car-
bon (OC) and concomitant organic matter (OM) content, and ionic species. $PM_{2.5}$ mass was measured at the T1 site, while PM_{10} was measured nearby. These mass measure-
ments, particularly the $PM_{2.5}$ measurement, are used to estimate the dust content of the aerosol, as will be explained below.
20   A Sunset Labs OCEC instrument (Birch and Cary, 1996; Doran et al., 2007a, b), us-
ing a thermo-optical technique, provided measurements of OC and EC. The instrument essentially provided 1-h sample with a detection limit of 0.02 μgCm^{-3} and an estimated uncertainty of 0.2 μgCm^{-3}. The organic carbon concentration was converted to organic matter concentration by multiplying by the factor 1.6, so that OM=1.6 OC. The value of
25 this conversion factor is fluid (Turpin and Lim, 2001; Malm et al., 2005; DeCarlo et al., 2008) and probably depends on the type of organic aerosol considered. For urban ar-
eas, Turpin and Lim (2001) argue that 1.6 (±0.2) is the most appropriate value. Using data collected from aircraft flights in the MCMA area, DeCarlo et al. (2008) found that

Closure on the single scattering albedo

J. C. Barnard et al.

Full Screen / Esc

Printer-friendly Version

Interactive Discussion

the OM/OC ratio varied from 1.6 to 2.3, with the lower values corresponding to air over the city, and larger values being associated with aged regional air. Considering these studies, we assume a value of 1.6.

Inorganic ionic species (e.g., Na^+, K^+, Ca^{2+}, Mg^{2+}, Cl^-, NO_3^-, NO_2^-, SO_4^{2-}) were measured with a PILS instrument (Orsini et al., 2003; Weber et al., 2001). The PILS instrument uses a small amount of water vapor to form water droplets around individual aerosol particles, dissolving water soluble components. The water is collected and analyzed using ion chromatography. This analysis cycle takes about four minutes, thereby producing a semi-continuous time series of aerosol inorganic ionic species. The uncertainty of these measurements is stated as ±10% (Weber et al., 2001).

$PM_{2.5}$ was observed at the T1 site by a tapered element oscillating microbalance (TEOM) instrument, with an estimated uncertainty of ±5%. PM_{10} was not measured at T1, but was at the Red Automática de Monitoreo Atmosférico (RAMA, http://www.sma.df.gob.mx/simat/pnrama2.htm) Villa de las Flores (VIF) site about 12 km southwest of T1. Figure 3 shows the various mass measurements averaged over the diurnal cycle. That is, for first hour of the day, extending from 00:00 LT to 01:00 LT (LT=UTC − 6 h), all mass measurements during this hour interval are averaged and so on for the other hours of the day. These averages are found over a time period extending from day 74 (15 March 2006) to day 87 (28 March 2006). For the purposes of this plot, the mass of all inorganic ionic species is lumped together under the banner "inorganics". The line labeled "fine mode dust" is found by subtracting all known substances (BC, OM, and inorganics) from the $PM_{2.5}$ mass and assuming that this residual is dust. Although we cannot be sure that this remainder is dust, we note that a considerable amount of dust was often witnessed at the T1 site.

Figure 3 reveals several interesting features. The first of these is the correlation between the $PM_{2.5}$ and PM_{10} masses. In particular, two peaks are seen in these concentrations, one occurring in the morning at about 09:00 LT and the other in late afternoon about 17:00 LT. The morning concentration maximum is caused by emissions into a shallow, stable boundary layer, where they are trapped, thereby increasing the mass

Closure on the single scattering albedo

J. C. Barnard et al.

Title Page

Abstract | Introduction

Conclusions | References

Tables | Figures

|◀ | ▶|

◀ | ▶

Back | Close

Full Screen / Esc

Printer-friendly Version

Interactive Discussion

concentration. The maxima in mass concentrations form just prior to the development of a convective boundary layer, which scours material from near the surface, resulting in a mass decrease. Such early morning concentration maxima also are seen in some of the individual chemical species, BC and OM. The late afternoon maxima in $PM_{2.5}$ and PM_{10} likely are caused by windblown dust (Querol et al., 2008).

Second, it must be noted that the morning peak in inorganic concentration occurs about an hour later than the morning maxima of BC and OM. The two species that most contribute to the inorganic peak around 10:00 LT are sulfate (SO_4) and nitrate (NO_3). Such a peak has been observed in these species at the MILAGRO T0 site (Paredes-Miranda et al., 2008) – a station fully in the urban core of the MCMA. Paredes-Miranda et al. (2008) suggest that the maximum in NO_3 occurs later in the day than primary emissions (e.g., BC) because most of the NO_3 is produced by same-day photochemical processes, obviously dependent on sunlight.

The relative humidity (RH) at the site was low during the day (Doran et al., 2007a, plots RH for the T2 site) generally ranging between about 10% and 40%, with larger RH occurring towards the last week of the campaign, when rain showers occurred. Accordingly we assumed that the aerosols at the surface were dry during most of the campaign. The assumption of a dry aerosol is supported by the work of Moffet et al. (2008a, b), who used single particle mass spectrometry (an aerosol time-of-flight mass spectrometer, ATOFMS) to analyze aerosol chemical and radiative properties, and noted that the radiative microphysical properties displayed no detectable RH dependence, thus suggesting that the particles were dry.

The chemical and optical measurements used in our closure study are summarized in Table 1.

2.4 Aerosol size distribution

Surface aerosol size/volume distribution data were not available at the T1 site because of instrument malfunctions. Without actual surface measurements of the size distribution, we assume that it can be approximated by a columnar distribution, derived from

Title Page

Abstract | Introduction

Conclusions | References

Tables | Figures

◄ | ►

◄ | ►

Back | Close

Full Screen / Esc

Printer-friendly Version

Interactive Discussion

the columnar AERONET volume distribution. This volume distribution is composed of two log-normal shapes (Dubovik et al., 2002):

$$\frac{dV}{d\ln r} = \frac{C_{V,f}}{\sqrt{2\pi}\sigma_f}\text{Exp}\left[-\frac{\log(r/r_{V,f})^2}{2\sigma_f^2}\right] + \frac{C_{V,c}}{\sqrt{2\pi}\sigma_c}\text{Exp}\left[-\frac{\log(r/r_{V,c})^2}{2\sigma_c^2}\right] \quad (1)$$

where V is the aerosol volume per unit volume of air (with units cm^3/cm^3), r is the aerosol radius, $C_{V,f}$ ($C_{V,c}$) is the fine (coarse) mode aerosol volume per unit volume of air, and $r_{V,f}$ ($r_{V,c}$) and σ_f (σ_c) are the fine (coarse) mode volume median radius and the standard deviation, respectively. The details of the coarse mode do not influence the results of our investigation to any material degree, because of the line and inlet loss mentioned in Sect. 2.2, although knowledge of the coarse mode volume distribution permits the estimation of the coarse mode on the magnitude of ϖ_0, as will be discussed in Sect. 3.5.

The shape parameters of the log-normal distributions, which are the volume mean radii and the standard deviations, are obtained from AERONET inversions based on irradiances measured by the CIMEL sun photometer deployed at the T1 site, averaged over the length of the deployment. Specifically, these values are $r_{V,f}$=0.156 μm, σ_f=0.465, $r_{V,c}$=3.41 μm, and σ_c=0.596. To what extent these values represent the size distribution at the surface is difficult to determine. However, some independent confirmation is available from size distribution measurements obtained from a Passive Cavity Aerosol Spectrometer Probe (PCASP). This instrument measures particles in a diameter range of 0.1 to 3.0 μm, and was deployed on the G-1 aircraft. Considering two over-flights over the T1 site at an altitude of about 500 m above the ground, fine mode volume distributions derived from the PCASP have an average $r_{V,f}$ equal to 0.151 μm and an average σ_f equal to 0.302, suggesting that the assumed surface size distribution is a least approximately correct.

The coefficients $C_{V,f}$ and $C_{V,c}$ are found by converting the mass in the fine and coarse modes to fine and coarse mode volumes. Each aerosol constituent is measured as a mass per unit volume of air, m, (with units μg/m^3), and these are converted to volumes

Closure on the single scattering albedo

J. C. Barnard et al.

Title Page

Abstract	Introduction
Conclusions	References
Tables	Figures

|◀ | ▶|

◀ | ▶

Back | Close

Full Screen / Esc

Printer-friendly Version

Interactive Discussion

by dividing by the constituent density. Summing over all constituents yields the volume in fine and coarse modes. For example, the fine mode volume, denoted as $V_{PM_{2.5}}$, is given by the relationship:

$$V_{PM_{2.5}} = \frac{m_{EC}}{\rho_{EC}} + \frac{m_{OM}}{\rho_{OM}} + \frac{m_{dust}}{\rho_{dust}} + \sum_{inorganics} \frac{m_i}{\rho_i} \tag{2}$$

where ρ_k is the density of the species "k" (e.g., EC, OM, dust, or inorganics). These densities are listed in Table 2. A similar relationship holds for the coarse mode volume. We then solve for the coefficients $C_{V,f}$ and $C_{V,c}$ using a system of two equations:

$$C_{V,f} \int_{r=0}^{r=1.25/\sqrt{\rho_{ave}}} \frac{1}{\sqrt{2\pi}\sigma_f} \mathrm{Exp}\left[-\frac{\ln(r/r_{V,f})^2}{2\sigma_f^2}\right] dr + C_{V,c} \int_{r=0}^{r=1.25/\sqrt{\rho_{ave}}} \frac{1}{\sqrt{2\pi}\sigma_c} \mathrm{Exp}\left[-\frac{\ln(r/r_{V,c})^2}{2\sigma_c^2}\right] dr = V_{PM_{2.5}} \tag{3}$$

$$C_{V,f} \int_{r=1.25/\sqrt{\rho_{ave}}}^{r=5.00/\sqrt{\rho_{ave}}} \frac{1}{\sqrt{2\pi}\sigma_f} \mathrm{Exp}\left[-\frac{\ln(r/r_{V,f})^2}{2\sigma_f^2}\right] dr + C_{V,c} \int_{r=1.25/\sqrt{\rho_{ave}}}^{r=5.00/\sqrt{\rho_{ave}}} \frac{1}{\sqrt{2\pi}\sigma_c} \mathrm{Exp}\left[-\frac{\ln(r/r_{V,c})^2}{2\sigma_c^2}\right] dr+ = V_{PM_{10}} - V_{PM_{2.5}}$$

In this equation, we explicitly note that aerodynamic diameter associated with $PM_{2.5}$ and PM_{10} measurements, is different from physical diameter, needed for radiative transfer calculations. The relationship between the two diameters is discussed in Shaw et al. (2008), and is expressed as $r_{physcial} = r_{aerodynamic}\sqrt{\chi/\rho}$, where χ is the particle shape factor, and ρ is the particle density. In general, both the shape factor and particle density are not well known for a collection of particles, and approximations are necessary, as follows. We assume that the shape factor is equal to one (i.e., spherically shaped particles), and for the density, we assume an average particle density, ρ_{ave}, of 1.9 g/cm^3, calculated from typical species mass concentrations and the densities listed in Table 2. Conversion of the volume distribution to a size distribution, $dn(r)/dr$, follows the usual formula, $dV/d\ln r = r(4/3\pi r^3)dn(r)/dr$. We acknowledge that this surface size distribution, derived from a columnar distribution, may be somewhat in error.

Closure on the single scattering albedo

J. C. Barnard et al.

Title Page

Abstract	Introduction
Conclusions	References
Tables	Figures

◀◀ ▶▶

◀ ▶

Back Close

Full Screen / Esc

Printer-friendly Version

Interactive Discussion

2.5 The WRF-Chem "chemical-to-optical properties" module

The WRF-Chem CTOM receives size-resolved chemical mass concentrations, and converts this information into aerosol optical properties. These properties include the aerosol extinction, $\sigma_{e,\lambda}$, with units 1/length; the single scattering albedo, $\varpi_{0,\lambda}$; the
5 aerosol scattering asymmetry factor, g_λ; and the aerosol backscatter coefficient, $\sigma_{b,\lambda}$. All of these optical properties are functions of the wavelength, and are computed explicitly at wavelengths of 300, 400, 600, and 1000 nm. For these calculations, the particles are assumed to be spherical. Unless otherwise noted, the wavelength of the calculations presented here is 870 nm, and from henceforth we will drop the subscript
10 "λ" from the optical variables. Because the CTOM did not calculate explicitly the optical properties at 870 nm, linear interpolation between 600 and 1000 nm was used to find the optical parameters at this wavelength.

The conversion of chemical information to optical information is a many-step process. The first step is specifying the size distribution. When operated within the full
15 WRF-Chem model, the CTOM receives aerosol chemical and size information from the aerosol chemistry model, MOSAIC (Zaveri et al., 2008). The MOSAIC model segregates the aerosols into size bins using a sectional approach, creating a discrete size distribution. Each bin contains an internally mixed aerosol with species mass concentration as determined by both emissions and MOSAIC. Our particular simulations use
20 eight size bins. The midpoint radius of a bin depends somewhat on the water content of the aerosol, but for dry aerosols, the nominal midpoint radii, defined as the geometric mean of the lower bin and upper bin limits, ranges from about 0.0276 μm for the smallest sizes, and increases exponentially up to about 3.5 μm. For each bin, the mass concentrations of each chemical species are converted to species volumes, by
25 dividing by the species density, a process analogous to that described in Eq. (2). For each bin, the volumes are summed, and from this total species volume, the number of particles is calculated, consistent with the bin size. The aerosol number densities in each of all eight bins compose the size distribution.

Next, for each size bin we need to find a refractive index. Given that the aerosols are assumed to be internally mixed, the oft-used volume averaging (Lesins et al., 2002) can be used to find the bulk refractive index for a bin. Volume averaging has been criticized because it may artificially inflate absorption (Bond et al., 2006). To avoid

5 this potential problem, an option is provided in the WRF-Chem CTOM to calculate the aerosol optical properties using a shell-core model (Bond et al., 2006; Ackerman and Toon, 1981), which places the BC as the spherical core, surrounded by a spherical shell composed of all the other species. The BC core is assigned a refractive index, and volume averaging of the remaining constituents is used to find the refractive index

10 of the shell. The refractive indices used in this study, as well as some of the sources of these values, are listed in Table 2.

Once the aerosol morphology is decided – shell/core versus volume mixing of BC – it is applied to all bins, and refractive indices are calculated for each bin. Armed with the number of particles in each bin, the size distribution, and the refractive index of

15 each bin, Mie calculations (or approximation thereof) are used to find the aerosol optical properties. In the CTOM, there are two options for performing these calculations. The first of these is a full-blown Mie calculation without any approximation. This option can be used with either the volume averaged refractive indices, or the shell/core configuration. Second, an approximation of Mie calculations, economized using Chebyshev

20 polynomials, is also available (Ghan and Zaveri, 2007). This approximation runs significantly quicker than the Mie algorithm and produces aerosol optical properties that do not differ significantly from the Mie scheme. For the calculations presented here, we use a shell/core configuration combined with the exact Mie calculation option.

We reiterate that, when used in a stand-alone mode, the CTOM does not take chemi-

25 cal mass information from the MOSAIC model, but relies on external input. For the evaluation described here, this external input consists of actual measurements of species mass and size distributions. This information is used to apportion aerosol mass over six of the eight size bins of the CTOM. For bins seven and eight, which would normally contain the largest particles, the aerosol mass is set equal to zero so that the calcula-

tions will be comparable to the observations, which are subject to an effective cut-off size of aerodynamic diameter of 2.5 μm, as mentioned above. For bins one through six, which contain the smallest particles, the mass fraction of any given aerosol species is assumed to be the same in each bin. To find the number of particles in a bin, the

5 volume distribution represented by Eq. (1) is converted to a size distribution, and the distribution is integrated between the lower and upper bin limits.

2.6 The modal module

As an independent check on the CTOM, we developed a module separately, which takes chemical mass input and size distribution information, and computes aerosol op-

10 tical properties, using an entirely modal approach with the aerosol volume distribution given by Eq. (1). Mass is distributed uniformly in the fine mode, so that the mass percentage for each species is the same, regardless of aerosol size. A shell/core configuration is assumed, with a specified refractive index for the EC core, and volume averaged refractive index for the shell. Although a coarse mode is included in the

15 modal module, this mode is not used in most calculations to ensure compatibility with the measurements. (The coarse mode is invoked, however, to determine how much this mode contributes to the value of ϖ_0, as discussed in Sect. 3.5.) Once the size distribution and refractive indexes are found, a Mie algorithm, integrated between radii of 0.01 and $1.25/\sqrt{1.9}\,\mu$m, is used to find the aerosol optical properties.

20 # 3 Results

3.1 Single-scattering albedo calculations versus observations

We present here the observed ϖ_0, and calculations of the same obtained from the modal model and the CTOM. For each of these methods, the aerosol chemical input and size distribution is obtained from the MILAGRO measurements. The CTOM uses

a sectional approach, while for the modal model, the size (or equivalently, volume) distribution is continuous. The continuous volume distribution is integrated over the width of each sectional bin to determine the amount of mass to be placed in that bin. The mass percentage of a particular constituent is the same for all bins.

Time series of ϖ_0 values at 870 nm, obtained from the CTOM, the modal module, and the measurements, are shown in Fig. 4. This figure covers the period over which ϖ_0 measurements were available, extending from Julian day 74 (15 March) to day 86 (27 March). Note that the calculated ϖ_0 values from the CTOM and the modal model closely follow each other throughout the period, and yield overall average values of ϖ_0 of 0.75 for both methods. This close correspondence suggests that: (1) the coding of the CTOM is likely to be correct, because the two methods were conceived independently of one another; and (2) the eight bin sectional representation in the CTOM provides adequate size resolution. When compared to the observations, we see that the diurnal behavior of the observed ϖ_0 is approximately captured by the calculations. Over the entire period, the averaged observed ϖ_0 is 0.77, which is very close to the averages obtained from the modal and CTOM calculations. Marley et al. (2009) report a mean observed value of ϖ_0 at 550 nm of 0.68 at the T1 site. This value is lower than that measured at 870 nm suggesting enhanced absorption at the lower wavelengths, perhaps attributable to dust (Bergstrom et al., 2007) or organic carbon (Barnard et al., 2008; Kirchstetter et al., 2004). Recall that the estimated uncertainty of the measured ϖ_0 is 6%, corresponding to an absolute uncertainty of 0.05. Because the calculated values, both 0.75, fall in the range 0.77 (measured) ±0.05, we can say at least for the mean value of ϖ_0, that closure is achieved without even having to evaluate the uncertainty of the calculations. The uncertainties in the simulations will be discussed in Sect. 3.3.

The ability to calculate a mean ϖ_0 close to the observed average is a good achievement; however, it is enlightening to investigate these results further by examining the two components that define ϖ_0. Specifically, ϖ_0 is defined as $B_{scat}/(B_{abs}+B_{scat})$, where B_{abs} and B_{scat} are the absorption and scattering coefficients, respectively. If the calcu-

Printer-friendly Version

Interactive Discussion

Closure on the single scattering albedo

J. C. Barnard et al.

lations are finding ϖ_0 for the "right reasons", then the calculations should predict each of these two components well. Figure 5 shows times series of these quantities. For B_{scat} the two sets of calculations agree quite well with one another, but are somewhat larger than the observations. The B_{scat} values, averaged over the length of the time series, are 33.3, 34.5, and 36.7 Mm^{-1}, for the observations, the modal technique, and the CTOM, respectively. Because the estimated uncertainty of the scattering measurements is a least 15%, corresponding to an absolute uncertainty of 5.0 Mm^{-1} in the observed averaged of 33.3 Mm^{-1}, we again find that closure is achieved between the observations and each of the two calculation methods, for the mean values of B_{scat}.

We now focus on B_{abs} (lower panel of Fig. 5). For this property, the propensity of the models to over-predict the observations is evident. This is illustrated in the averages, which are 9.2±0.9, 12.6, and 13.8 Mm^{-1}, for the observations, the modal technique and the CTOM, respectively. The "±0.9" appended to the observed value indicates the estimated uncertainty of 10% in PAS absorption measurements. As discussed above, we found that the mean values of ϖ_0 are slightly less for the calculations (0.75) than for the observations (0.77). Apparently, the larger calculated values of B_{abs} are causing this difference. We will remark more on the discrepancy between calculated and observed B_{abs} values below.

3.2 Physical determinants of ϖ_0

Following the lead of Paredes-Miranda (2008), significant clues about the physical and chemical determinants of aerosol optical properties can be gleaned by examining the diurnal variation of these properties, where the average at each hour is found, similar to the calculations performed in generated Fig. 3 above. Figure 6 shows these averages for ϖ_0, B_{abs}, and B_{scat}, for the observations (solid blue line), the modal model (solid red line), and the CTOM (dashed red line). The top panel shows ϖ_0 and we see that both calculations do a fairly good job of simulating the diurnal variation of the ϖ_0. Although the difference in mean values between observations and simulations of B_{scat} are small, the observed diurnal behavior for B_{scat} (middle panel) is only weakly simu-

lated by the calculations. For B_{abs} (lower panel), however, the calculated values exceed the observations as expected, but the essence of the diurnal variation is captured.

It is interesting to compare the observations of B_{abs} and B_{scat}, at the urban Mexico City T0 site (Paredes-Miranda, 2008) with the T1 observations presented in Fig. 6. For each site, the coarse aerosol mode is not measured, which makes the comparison more secure. However, the wavelengths of the absorption and scattering measurements are different at each site, 532 nm at the T0 site versus 870 nm at the T1 site, which makes the comparison slightly more difficult, because, for example, dust and organic aerosol might absorb at 532 nm but not absorb at 870 nm (Barnard et al., 2008). First, we note that B_{abs} at both sites shows a similar diurnal variation, peaking at around 06:00 LST, corresponding to the peak value of BC (see Fig. 3). This absorption peak is another manifestation of the emission of absorbing substances, primarily BC, into the late evening stable boundary layer, followed by the scavenging action of the convective boundary layer to produce a maximum in BC values. Second, in contrast to the similarities in absorption behavior between the T0 and T1 sites, there is a significant difference in the diurnal variation of B_{scat} at each site. At T0 this quantity peaks at around 10:00 LT and then declines for the remainder of the day. However, at T1, although there is an increase in scattering at 10:00 LT, after this time, B_{scat} remains essentially flat, and does not decline significantly until about 18:00 LT.

To investigate what might contribute to this midday plateau in scattering, we refer back to Fig. 3, which displays the diurnal variation of $PM_{2.5}$, PM_{10}, and chemical constituents of $PM_{2.5}$ mass, which includes BC, OM, inorganics, and dust. Clearly, at the start of the daylight hours, around 06:00 LT, the mass concentrations of all these species are significant, and all species contribute to B_{scat}. In terms of mass, dust is most important at this time. As the day progresses, dust and BC assume less importance, but after about 15:00 LT, dust is again the largest fraction of $PM_{2.5}$ mass. Coarse mode dust, crudely represented by the PM_{10} mass, also plays a very important role in determining the scattering, as will be discussed below. Unlike the T0 site, where secondary organic aerosol formation plays the prominent role in determining the scattering

in the midday hours, at the T1 site, dust appears to be the major factor that influences scattering.

3.3 Sensitivities and uncertainties

The discrepancies between calculated and observed diurnal values of B_{abs} and B_{scat}
can be attributed initially to several causes. The first of these, and perhaps the most important, is the imperfect knowledge of the mass concentrations of the chemical species that are the starting point of these calculations. Second, once the chemical mass constituents are measured, it is necessary to convert this information to particle refractive index. This process requires assumptions about the density and refractive index about each chemical species. Third, we assume that the particles are internally mixed and are of spherical shape, with a shell core morphology where BC is surrounded by the shell. Finally, errors in specification of the size distribution can greatly influence the outcome of the calculations.

Some of these issues, for example, the assumption of spherical particle shape, are necessary to allow traditional Mie calculations. Methods of finding optical properties of non-spherical particles exist, but implementing these approaches are beyond the scope of this paper, as well as currently being impractical to implement in WRF-Chem. Because of these difficulties, we concentrate on possible sources of error that are likely to be large: errors in the input chemical masses, and the conversion of chemical masses to particle refractive index. The effect of an error of a certain variable (e.g., $PM_{2.5}$) can be uncovered by examining how the optical properties change when the variable is perturbed. To this end, we show the results of this sensitivity study, in which changes in ϖ_0, B_{abs}, and B_{scat} are tabulated in response to a systematic perturbation of variables by 10%. The results of this sensitivity study are shown in Table 3.

The first column in this table is the quantity that is varied, while the other three columns show the change caused by this variation. For example, if the BC mass concentration is increased by 10%, B_{abs} increases by 1.74 Mm^{-1}. The boldface numbers in a given column emphasize the four largest changes for the optical property in ques-

Closure on the single scattering albedo

J. C. Barnard et al.

Full Screen / Esc

Printer-friendly Version

Interactive Discussion

tion. Most of these particular sensitivities are not surprising; e.g., changes in the real part of the refractive indices for dust, inorganics, and OM dramatically influence B_{scat}.

Some of the variables have parallel, correlated effects on the optical properties. For example, increasing either the BC mass concentration or the imaginary part of the BC refractive index will increase absorption, and our sensitivity testing only tells us that both of these factors are important in determining B_{abs}, but we cannot unambiguously determine which of these two variables might actually be most important in causing the difference between calculated and observed values. Additionally, for these sensitivity tests, we have not considered species densities because the effect of density variations is completely parallel to changes in mass concentrations. Bond and Bergstrom (2006) delineate the probable uncertainties in BC density, ranging from 1.7 to 1.9 g/cm^3. From the putative value of 1.8 g/cm^3, these values represent about a ±6% variation. For the other constituents, such as OM, the variation is likely to be higher, and we therefore assign an uncertainty of ±10% to these compounds.

The sensitivities listed in Table 3, along with estimated uncertainties of the variables, form the basis of improving the agreement between the optical property simulations and observations. Unfortunately, the uncertainties of some of the variables are not known well, and we must rely on educated guesses. Uncertainties, such as those for BC and OM are obtained from the manufacturer of the OC/EC instruments, as mentioned above. (For OM, we multiplied the OC uncertainty of 0.2 μg/m^3 by 1.6, the conversion factor between OC and OM.) The uncertainties for the BC optical properties are in a range thought plausible, as discussed in Bond and Bergstrom (2006). Ranges of the real part of the refractive index, n, for various organic compounds are reviewed in Kanakidou et al. (2005), and the range extends from about 1.35 to 1.75; however, most compounds fall in a smaller interval, from 1.40 and 1.55. Accordingly, we take the uncertainty for OM to be ±5%. We arbitrarily assign this level of uncertainty to n for inorganic compounds. For refractive index of dust, we examine the range of values given in Mishra and Tripathi (2008), Prasad and Singh (2007), and Clarke et al. (2004) and assign uncertainties of ±5% and ±100% for the real and imaginary components,

respectively. In Prasad and Singh (2007), the imaginary component for dust ranges from 0.001 to 0.008 thus leading to a large uncertainty. Because the bulk of the dust is found in the coarse mode, which does not influence aerosol optical properties as much as the fine mode, this level of uncertainty does not significantly affect the results presented here.

3.4 Can closure be achieved for hourly values?

Given the uncertainties and sensitivities listed in Table 3, several approaches can be applied to reconcile the diurnal observations and calculations. Following the traditional path of a closure study (Quinn et al., 1996), one can determine if the optical properties agree within established uncertainties for the observations and the calculations. We take another approach here and in the spirit of an optimization process, we systematically adjust the variables, with their uncertainty limits, to achieve the closest agreement between the observations and calculations. This process is made easier by a careful selection of variables to adjust. Recall that the modal model and the CTOM both overpredict the average value of B_{abs} while the average value of B_{scat} is predicted reasonably well. With this in mind, we can select from Table 3 a subset of variables that act most strongly to achieve the desired reduction in the calculated value of B_{abs}, while not significantly affecting B_{scat}.

To achieve reductions in calculated B_{abs} values, the greatest effect comes from, as expected, reducing the BC mass and the imaginary part of the BC refractive index, k. Secondary reductions occur by lowering the real part of the refractive index, n, for inorganics and dust. With these factors in mind, we lower both the BC mass concentration and k within the specified uncertainty limits and perform the calculations again. The results of this procedure are shown in Fig. 7, along with the estimated uncertainties in B_{abs}, B_{scat}, and ϖ_0, shown as the blue error bars. This figure shows that on an hour-by-hour basis, closure is achieved for most of the day for ϖ_0. Closure is evident for B_{abs} except for the hours in the late evening and early morning. The absence of agreement between the hours of 00:00 LT and 06:30 LT is particularly strik-

Printer-friendly Version

Interactive Discussion

Closure on the single scattering albedo

J. C. Barnard et al.

ing. We speculate that this lack of closure could possibly be caused by a violation of the internal mixing assumption, inherent in the modal approach and the WRF-Chem CTOM. Based on a detailed examination of individual particles sampled in the Mexico City plume, Adachi and Buseck (2008) assert that the internal mixing assumption is "relatively reliable for modeling". Doran et al. (2008) find that at the T1 site, coating of BC particles progresses rapidly during the daylight hours, but is limited or even absent during the night. These two studies suggest a picture where fresh BC emissions in the early morning would tend to be externally mixed, and then become quickly internally mixed after the sun rises. Because the specific absorption of unmixed BC is much lower than that of mixed BC, invoking the internally mixed assumption throughout the diurnal cycle would tend to overestimate the absorption during the early morning hours, particularly before sunrise, as observed in Fig. 7. A quantitative estimate of the difference in absorption between uncoated and coated BC particles is obtained from BC specific absorption measurements taken at the T1 site, as discussed in Doran et al. (2008). For the nighttime hours, the specific absorption values (870 nm) are about 5 m^2/g, while during the day, the values exceed 7 m^2/g, and a crude estimate of the ratio of daytime absorption to nighttime absorption would be 5/7, or 0.7. We note that if we multiply the modeled absorption between the hours of 00:00 and 06:00 LST, by this factor, the agreement between the modified, modeled B_{abs} and the measured B_{abs} becomes much better. Specifically, the average unmodified absorption in the interval 00:00 to 06:00 LST is 12.3 Mm^{-1} and 13.6 Mm^{-1} for the modal and CTOM approaches, respectively, and these values are reduced to 8.71 Mm^{-1} and 9.63 Mm^{-1} after multiplication by 5/7, much closer to the averaged observed value of 9.21 Mm^{-1} (averaged in the time interval 00:00 LT to 06:00 LT).

Closure between observed and calculated B_{scat} diurnal values seems particularly problematic, as observed in the middle panel of Fig. 7, although both modeling techniques capture the basic diurnal cycle – lower scattering in the early morning hours (before 08:00 LT) and late evening hours (after 18:00 LT), and significantly greater scattering during midday. We could, of course, vary the refractive indices, etc. of the var-

Full Screen / Esc

Printer-friendly Version

Interactive Discussion

ious aerosol components to achieve closure during some parts of the day, but when this done, the difference between observations and modeling results becomes worse during the other parts of the day. We speculate that some of the discrepancy between observed and calculated values of B_{scat} could be caused by large dust particles, which may be smaller than the estimated cut-off value of 2.5 μm aerodynamic diameter, but nevertheless large enough to skew the size distribution towards larger sizes during the times that dust is abundant. That windblown dust is an important factor at T1 has been discussed by Querol et al. (2008); in particular, we note that the mean values of $PM_{2.5}$ (33 μg/m^3) and PM_{10} (80 μg/m^3) are the largest observed over a sampling network in the MCMA, and that local soil resuspension was a major contributing factor to these large mass loadings (as was visually observed at the T1 site by the authors). If we temporarily vary $r_{V,f}$ in Eq. (3) over a range of ±20%, so that it is larger during the daylight hours, and smaller during the nighttime hours, then the simulations capture the diurnal variation in B_{scat} very well, suggesting that larger particles – primarily windblown dust – are more abundant during the day. Additionally, when large particles are present, errors in scattering measurements may be amplified, because of problems in correcting for the forward scattering, which is not sensed by the scattering measurement. The presence of windblown dust is particularly acute during the afternoon hours, when the winds are generally the strongest, and we note in Fig. 7 that the observed scattering has a secondary peak in the afternoon, perhaps in response to windblown dust. The peak that occurs around 09:30 LT probably can be attributed to dust, as well as the formation of secondary aerosol species, as discussed in Sect. 2.3.

Finally, Table 4 lists the "optimized" average values of ϖ_0, B_{scat}, and B_{abs}, over the period extending from 15 through 27 March. Generally speaking, the agreement between the observations and calculations is good and within the estimated systematic uncertainties of the measurements, except for B_{abs} (CTOM). Thus, after adjustment, closure is achieved for all mean aerosol properties and the calculations, except for the CTOM calculation of B_{abs}. This residual discrepancy may be caused, in part, by the internal mixing assumption inherent to the CTOM (although this assumption is also part

of the modal approach).

3.5 To what extent does the coarse mode influence the value of ϖ_0?

Given that dust may significantly influence optical properties at the T1 site, we ask: to what extent does the coarse mode contribute to ϖ_0? If the contribution is significant,
⁵ the use of fine-mode ϖ_0 values in radiative transfer models may produce erroneous irradiance calculations. Using the volume distribution depicted by Eq. (1) and the volume distribution parameters discussed in Sect. 2.4 ($r_{V,f}$=0.156 μm, σ_f=0.465, $r_{V,c}$=3.41 μm, σ_c=0.596), we can estimate the effect of the coarse mode by using the volume (size) distribution to calculate ϖ_0 with and without the coarse mode. The volume distribution
¹⁰ also requires the volume concentration parameters, $C_{V,f}$ and $C_{V,c}$. For these, we take the average values of these parameters over the length of the campaign at site T1. The values are 0.03 and 0.098 cm^3/cm^3 for $C_{V,f}$ and $C_{V,c}$, respectively. These values imply a lot of mass in the coarse mode. We can calculate the ratio, PM$_{2.5}$/PM$_{10}$, from the volume distribution, assuming that only dust exists in the coarse mode, and the ratio
¹⁵ is about 0.52. Actual surface measurements of PM$_{2.5}$ and PM$_{10}$ mass concentrations, when averaged over most of the month of March 2006 (Querol et al., 2008), yield a ratio of 0.41 (=33 μgm^{-3}÷80 μgm^{-3}), roughly consistent with that derived from the volume distribution. We can certainly assert that at the T1 site, there is a lot of aerosol mass in the coarse mode!
²⁰   For the conversion of mass to optical properties, we assume that the coarse mode consists entirely of dust, with a refractive index of 1.55+0.004i, while the fine mode contains dust, BC, and other chemical species. We simply assign a refractive index of 1.55+0.04i to the fine mode (aerodynamic diameters from 0.0 μm to 2.5 μm); this refractive index produces a fine mode ϖ_0 value of about 0.76 – very close to the ob-
²⁵ served fine-mode mean value of 0.77 at 870 nm. When the coarse mode is included in the calculations, ϖ_0 increases from 0.76 to 0.80, a change of 0.04, because of the contribution of coarse mode dust scattering to the overall scattering of the aerosol load. For particularly dusty days (e.g., 20 March 2006), the change can be as large as

Full Screen / Esc

Printer-friendly Version

Interactive Discussion

0.07. Such changes in ϖ_0 are significant, and would occur during the daytime when windblown dust is prevalent, and would therefore influence calculations of shortwave irradiances, heating rates, and photolysis rates.

3.6 The full WRF-Chem results

Recall that, for all the results presented above, the WRF-Chem CTOM was extracted from the model and run in a stand-alone offline mode, in which actual chemical mass concentration observations were used to drive the offline CTOM. Figure 8 shows diurnally averaged ϖ_0 values simulated by the full WRF-Chem model run in 3-D mode, which starts with emissions data, and then predicts the chemical concentrations at each grid point using the meteorological and chemical transport scheme embedded in the WRF-Chem model. In this figure, results of the full simulations are shown in red, while the observations are shown in blue. Clearly the full simulation fails to portray the diurnal variation of the observations, and mean value of the full simulations (0.90) is far different from that of the observations (0.77). It is difficult, and beyond the scope of this paper, to diagnose all contributing factors to this discrepancy. Of the many possible factors, however, one is not associated with the model itself, but rather the emissions that are an input to the model. Errors in emissions estimates will clearly contribute to erroneous model output. Fast et al. (2009) showed that BC was simulated reasonably well within the city at the T0 site, but the model usually underestimated BC at the T1 site, particularly between 05:00 and 10:00 LT. While errors in the vertical mixing could also affect BC concentrations, Fast et al. (2009) also showed that the predicted boundary layer depth was similar to measurements at T1 during the morning.

To test the hypothesis that BC emissions are not well characterized in the vicinity of the T1 site, we ran the full simulation again, the only difference being that the simulated BC values are replaced by the observed values at the T1 site. Results of this simulation are shown by the dashed red line in Fig. 8, and we see a noticeable improvement in the ability of WRF-Chem to predict ϖ_0; the re-calculated averaged ϖ_0 value is now 0.85. This test suggests that at least some of discrepancy between the full simulation and

the observations can be attributed to faulty BC emissions inputs. We note that WRF-Chem did produce a diurnally varying ϖ_0 similar to the observations at the T0 site (not shown) because the errors in the predicted BC were much smaller at that location.

Based on this closure study, we can conclude that the errors in the predicted ϖ_0
from the full WRF-Chem simulation can be attributed mostly to errors in the predicted aerosol composition and size distribution rather than on assumptions employed by the CTOM.

4   Conclusions

This study has focused on the ability of the WRF-Chem aerosol "chemical to optical properties" module (CTOM) to predict ϖ_0 at the T1 MILAGRO site. The CTOM was tested in the framework of a closure experiment, in which observed aerosol data, consisting of chemical mass measurements and estimated aerosol size distributions, were used as input to the CTOM, and the CTOM then used to calculate ϖ_0. Results of these calculations were then compared with ϖ_0 observations to determine if closure is achieved, with closure defined as agreement between the calculations and observations within the known uncertainty limits of the observations. A separate modal module was written, which was used to check on the adequacy of the sectional resolution within the WRF-Chem CTOM, as well as providing a check on the coding of the CTOM.

Observed ϖ_0 values were derived from scattering and absorption measurements obtained from a photoacoustic spectrometer, operating at a wavelength of 870 nm. Because of line and inlet losses, the spectrometer was only able to measure particles with aerodynamic diameters less than about 2.5 μm, and therefore the ϖ_0 values considered here are "fine mode" values. The comparison between observed and simulated values spanned the 12 days, from 15 through 27 March 2008. When averaged over this time span, the observed ϖ_0 value was 0.77 with an uncertainty of about 6% (±0.05). The simulated mean ϖ_0 values were 0.75, for both the CTOM and modal approach, and these values fall within the uncertainty of the measured ϖ_0 implying the achieve-

ment of closure. In terms of mean values, closure was also successful for the scattering coefficients, B_{scat} ; both CTOM and modal simulated values agreed (34.5 Mm^{-1}, and 36.7 Mm^{-1}) with the observed value within the 15% uncertainty of the scattering measurement, 33.3±5.0 Mm^{-1}. However, both the simulated CTOM and modal mean absorption coefficients, B_{abs}, exceeded the observed value; specifically, the mean values are 9.2±0.9, 12.6, and 13.8 Mm^{-1}, for the observed, modal and CTOM, respectively. When BC refractive mass concentrations, densities, and refractive indices are adjusted to within their known uncertainties, the new simulated B_{abs} values are 9.9 and 11.0 Mm^{-1}, for the modal and CTOM, respectively. In terms of mean B_{abs} values, closure is therefore achieved for the modal approach, but not for the CTOM.

We then examined the diurnal variation of the ϖ_0, B_{scat}, and B_{abs}, by plotting averages of these quantities over the entire time period of the campaign, for hourly intervals: 00:00–01:00 LT, 01:00–02:00 LT, up to 23:00–24:00 LT. The diurnal variation of ϖ_0 and B_{abs} is captured quite well; the observed minimum of ϖ_0 near 07:00 LT is simulated well by both the modal model and CTOM. This minimum corresponds to a maximum in B_{abs} and BC mass concentration, suggesting that BC mass concentration is the primary contributor to aerosol absorption at 870 nm. The observed diurnal variation in B_{scat} is not well simulated. The observations are low in the early morning, before sunrise, and then increase during the day to a plateau, only to fall again as night approaches. We speculate that the increase in scattering during the day could be caused, in part, by windblown dust, which would skew the size distribution towards larger particles, causing an increase in scattering.

Because we could only measure the fine mode aerosols, and because the dust content at the T1 site is so large (Querol et al., 2008), we estimated the effect of neglecting the coarse mode (aerodynamic diameter>2.5 μm) on the value of ϖ_0. We estimate that including the coarse mode would increase the mean value of ϖ_0 from 0.77 to 0.81, a difference of 0.04, but for especially dusty days, the increase could be much larger, 0.07. Increases of this magnitude would have a significant influence on irradiances calculated using radiative transfer models.

Closure on the single scattering albedo

J. C. Barnard et al.

Finally, a full WRF-Chem simulation, including the WRF-Chem meteorological, emissions, and chemical transport modules, is performed to determine how well the full model predicts ϖ_0. We find that the full simulation can neither simulate the diurnal variation well, nor can it predict the mean value; recall that the observed mean ϖ_0

5 value is 0.77, but the full WRF-Chem simulated value is 0.90, a difference of 0.13. We speculate that some of the discrepancy stems from the considerable difficulties in specifying emissions accurately. When the observed BC mass concentrations at T1 are substituted into the full simulation, replacing the simulated values derived from the emissions inventory estimates used as model input, the simulated mean value, 0.85,

10 now is much closer to the observed mean value, 0.77, and some of the diurnal variation is simulated. This test suggests that the accuracy of BC emission inventories affects the skill of the WRF-Chem model to properly simulate aerosol optical properties.

References

Ackerman, T. P. and Toon, O. B.: Absorption of visible radiation in atmosphere containing

25 mixtures of absorbing and non-absorbing particles, Appl. Optics, 20(20), 3661–3662, 1981.
Adachi, K. and Buseck, P. R.: Internally mixed soot, sulfates, and organic matter in aerosol particles from Mexico City, Atmos. Chem. Phys., 8, 6469–6481, 2008,
http://www.atmos-chem-phys.net/8/6469/2008/.

Andreae, M. O. and Gelencsér, A.: Black carbon or brown carbon? The nature of light-absorbing carbonaceous aerosols, Atmos. Chem. Phys., 6, 3131–3148, 2006, http://www.atmos-chem-phys.net/6/3131/2006/.

Arnott, W. P., Moosmüller, H., Rogers, C. F., Jin, J., and Bruch, R.: Photoacoustic spectrometer for measuring light absorption by aerosol: instrument description, Atmos. Environ., 33, 2845–2852, 1999.

Barnard, J. C., Volkamer, R., and Kassianov, E. I.: Estimation of the mass absorption cross section of the organic carbon component of aerosols in the Mexico City Metropolitan Area, Atmos. Chem. Phys., 8, 6665–6679, 2008, http://www.atmos-chem-phys.net/8/6665/2008/.

Bergstrom, R. W., Pilewskie, P., Russell, P. B., Redemann, J., Bond, T. C., Quinn, P. K., and Sierau, B.: Spectral absorption properties of atmospheric aerosols, Atmos. Chem. Phys., 7, 5937–5943, 2007, http://www.atmos-chem-phys.net/7/5937/2007/.

Birch, M. E. and Cary, R. A.: Elemental carbon-based method for monitoring occupational exposures to particulate diesel exhaust, Aerosol Sci. Tech., 25, 221–241, 1996.

Bond, T. C., Habib, G., and Bergstrom, R. W.: Limitations in the enhancement of visible light absorption due to mixing state, J. Geophys. Res., 111, D20211, doi:10.1029/2006JD007315, 2006.

Bond, T. C. and Bergstrom, R. W.: Light absorption by carbonaceous particles: An investigative review, Aerosol Sci. Tech., 40, 27–67, 2006.

Chaudhry, Z., Vanderlei Martins, J., Li, Z., Tsay, S.-C., Chen, H., Wang., P., Wen, T., Li, C., and Dickerson, R. R.: In situ measurements of aerosol mass concentrations and radiative properties in Xianghe, southeast of Beijing, J. Geophys. Res., 112, D23S90, doi:10.1029/2007JD009055, 2007.

Clarke, A. D., Shinozuka, Y., Kapustin, V. N., Howell, S., Huebert, B., Doherty, S., Anderson, T., Covert, D., Anderson, J., Hua, X., Moore II, K. G., McNaughton, C., Carmichael, G., and Weber, R.: Size distribution and mixtures of dust and black carbon aerosol in Asian outflows: Physiochemistry and optical properties, J. Geophys. Res., 109, D15S09, doi:10.1029/2003JD004378, 2004.

Cook, J., Highwood, E. J., Coe, H., Formenti, P., Haywood, J. M., and Crosier, J.: A comparison of aerosol optical and chemical properties over the Adriatic and Black Seas during summer 2004: Two case-studies from ADRIEX, Q. J. Roy. Meteorol. Soc., 133(S1), 35–45,

Closure on the single scattering albedo

J. C. Barnard et al.

doi:10.1002/qj.93, 2007.

DeCarlo, P. F., Dunlea, E. J., Kimmel, J. R., Aiken, A. C., Sueper, D., Crounse, J., Wennberg, P. O., Emmons, L., Shinozuka, Y., Clarke, A., Zhou, J., Tomlinson, J., Collins, D. R., Knapp, D., Weinheimer, A. J., Montzka, D. D., Campos, T., and Jimenez, J. L.: Fast airborne aerosol size and chemistry measurements above Mexico City and Central Mexico during the MILAGRO campaign, Atmos. Chem. Phys., 8, 4027–4048, 2008, http://www.atmos-chem-phys.net/8/4027/2008/.

Doran, J. C., Barnard, J. C., Arnott, W. P., Cary, R., Coulter, R., Fast, J. D., Kassianov, E. I., Kleinman, L., Laulainen, N. S., Martin, T., Paredes-Miranda, G., Pekour, M. S., Shaw, W. J., Smith, D. F., Springston, S. R., and Yu, X.-Y.: The T1-T2 study: evolution of aerosol properties downwind of Mexico City, Atmos. Chem. Phys., 7, 1585–1598, 2007, http://www.atmos-chem-phys.net/7/1585/2007/.

Doran, J. C.: Corrigendum to "The T1-T2 study: Evolution of aerosol properties downwind of Mexico City", Atmos. Chem. Phys., 7, 2197–2198, 2007b, http://www.atmos-chem-phys.net/7/2197/2007/.

Doran, J. C., Fast, J. D., Barnard, J. C., Laskin, A., Desyaterik, Y., and Gilles, M. K.: Applications of lagrangian dispersion modeling to the analysis of changes in the specific absorption of elemental carbon, Atmos. Chem. Phys., 8, 1377–1389, 2008, http://www.atmos-chem-phys.net/8/1377/2008/.

Dubovik, O., Holben, B., Eck, T. F., Smirnov, A., Kaufman, Y. J., King, M. D., Tanné, D., and Slusker, I.: Variability of absorption and optical properties of key aerosol types observed in worldwide locations, J. Atmos. Sci., 59, 590–608, 2002.

Fast, J. D, Gustafson Jr., W. I., Easter, R. C., Zaveri, R. A., Barnard, J. C., Chapman, E. G., and. Grell, G. A.: Evolution of ozone, particulates, and aerosol direct forcing in an urban area using a new fully-coupled meteorology, chemistry, and aerosol model, J. Geophys. Res., 111, D21305, doi:10.1029/2005JD006721, 2006.

Fast, J. D., Aiken, A. C., Allan, J., Alexander, L., Campos, T., Canagaratna, M. R., Chapman, E., DeCarlo, P. F., de Foy, B., Gaffney, J., de Gouw, J., Doran, J. C., Emmons, L., Hodzic, A., Herndon, S. C., Huey, G., Jayne, J. T., Jimenez, J. L., Kleinman, L., Kuster, W., Marley, N., Russell, L., Ochoa, C., Onasch, T. B., Pekour, M., Song, C., Ulbrich, I. M., Warneke, C., Welsh-Bon, D., Wiedinmyer, C., Worsnop, D. R., Yu, X.-Y., and Zaveri, R.: Evaluating simulated primary anthropogenic and biomass burning organic aerosols during MILAGRO: implications for assessing treatments of secondary organic aerosols, Atmos. Chem. Phys.

Closure on the single scattering albedo

J. C. Barnard et al.

Discuss., 9, 4805–4871, 2009,
http://www.atmos-chem-phys-discuss.net/9/4805/2009/.

Fiebig, M., Petzold, A., Wandinger, U., Wendisch, M., Kiemle, C., Stifter, A., Ebert, M., Rother, T., and Leiterer, U.: Optical closure for an aerosol column: Method accuracy, and inferable properties applied to a biomass-burning aerosol and its radiative forcing, J. Geophys. Res., 107(D21), 8130, doi:10.1029/2000JD000192, 2002.

Ghan, S. J. and Schwartz, S. E.: Aerosol properties and processes, B. Am. Meteorol. Soc., 88(7), 1059–1082, 2007.

Ghan, S. J. and Zaveri, R. A.: Parameterization of optical properties for hydrated internally mixed aerosol, J. Geophys. Res., 112(D10), D10201, doi:10.1029/2006JD007927, 2007.

Grell, G. A., Peckham, S. E., Schmitz, R., and McKeen, S. A., Frost, G., Skamarock, W. C., and Eder, B.: Fully coupled "online" chemistry within the WRF model, Atmos. Environ., 39, 6957–6976, 2005.

Heintzenberg, J., Charlson, R. J., Clarke, A. D., Liousse, C., Ramaswamy, V., Shine, K. P., Wendisch, M., and Helas, G.: Measurements and modeling of aerosol single-scattering albedo: Progress, problems, and prospects, Beitr. Phys. Atmos., 249–263, 1997.

Kanakidou, M., Seinfeld, J. H., Pandis, S. N., Barnes, I., Dentener, F. J., Facchini, M. C., Van Dingenen, R., Ervens, B., Nenes, A., Nielsen, C. J., Swietlicki, E., Putaud, J. P., Balkanski, Y., Fuzzi, S., Horth, J., Moortgat, G. K., Winterhalter, R., Myhre, C. E. L., Tsigaridis, K., Vignati, E., Stephanou, E. G., and Wilson, J.: Organic aerosol and global climate modelling: a review, Atmos. Chem. Phys., 5, 1053–1123, 2005,
http://www.atmos-chem-phys.net/5/1053/2005/.

Kirchstetter, T. W., Novakov, T., and Hobbs, P.: Evidence that the spectral dependence of light absorption by aerosols is affected by organic carbon, J. Geophys. Res., 109, D21208, doi:10.1029/2004JD004999, 2004.

Lack, D. A., Cappa, C. D., Baynard, T., Massoli, P., Covert, D. S., Sierau, B., Bates, T. S., Quinn, P. K., Lovejoy, E. R., and Ravishankara, A. R.: Bias in filter based aerosol absorption measurements due to organic aerosol loading: Evidence from ambient sampling, Aerosol Sci. Tech., 42(12), 1033–1041, 2008.

Lesins, G., Chyek, P., and Lohmann, U.: A study of internal and external mixing scenarios and its effect on aerosol optical properties and direct radiative forcing, J. Geophys. Res., 107(D10), 4094, doi:10.1029/2001JD000973, 2002.

Mallet, M., Roger, J. C., Despiau, S., Dubovik, O., and Putand, J. P.: Microphysical and optical

Closure on the single scattering albedo

J. C. Barnard et al.

Title Page

Abstract	Introduction
Conclusions	References
Tables	Figures

◄ | ►◄

◄ | ►

Back | Close

Full Screen / Esc

Printer-friendly Version

Interactive Discussion

properties of aerosol particles in urban zone during EXCOMPTE, Atmos. Res., 69, 73–97, 2003.

Malm, W. C., Day, D. E., Carrico, C., Kreidenweis, S. M., Collett, J. L., McMeeking, G., Lee, T., Carrillo, J., and Schichtel, B.: Intercomparison and close calculations using measurements of aerosol species and optical properties during the Yosemite Aerosol Characterization Study, J. Geophys. Res., 110, D14302, doi:10.1029/2004JD005494, 2005.

Marley, N. A., Gaffney, J. S., Castro, T., Salcido, A., and Frederick, J.: Measurements of aerosol absorption and scattering in the Mexico City Metropolitan Area during the MILAGRO field campaign: a comparison of results from the T0 and T1 sites, Atmos. Chem. Phys., 9, 189–206, 2009,
http://www.atmos-chem-phys.net/9/189/2009/.

Mishra, S. K. and Tripathi, S. N.: Modeling optical properties of mineral dust over the Indian Desert, J. Geophys. Res., 113, D23201, doi:10.1029/2008JD010048, 2008.

Moffet, R. C., Qin, X., Rebotier, T., Furutani, H., and Prather, K. A.: Chemically segregated optical and microphysical properties of ambient aerosols measured in a single-particle mass spectrometer, J. Geophys. Res., 113, D12213, doi:10.1029/2007JD009393, 2008a.

Moffet, R. C., de Foy, B., Molina, L. T., Molina, M. J., and Prather, K. A.: Measurement of ambient aerosols in northern Mexico City by single particle mass spectrometry, Atmos. Chem. Phys., 8, 4499–4516, 2008b,
http://www.atmos-chem-phys.net/8/4499/2008/.

Orsini, D. A., Ma, Y., Sullivan, A., Sierau, B., Bauman, K., and Weber, R. J.: Refinements to the particle-into-liquid sampler (PILS) for ground and airborne measurements of water soluble aerosol concentration, Atmos. Environ., 37, 1243–1259, 2003.

Paredes-Miranda, G., Arnott, W. P., Jimenez, J. L., Aiken, A. C., Gaffney, J. S., and Marley, N. A.: Primary and secondary contributions to aerosol light scattering and absorption in Mexico City during the MILAGRO 2006 campaign, Atmos. Chem. Phys. Discuss., 8, 16951–16979, 2008,
http://www.atmos-chem-phys-discuss.net/8/16951/2008/.

Pesava, P., Horvath, H., and Kasahara, M.: A local optical closure experiment in Vienna, J. Aerosol Sci., 32, 1249–1267, 2001.

Prasad, A. K. and Singh, R. P.: Changes in aerosol parameters during major dust storm events (2001–2005) over the Indo-Gangetic Plains using AERONET and MODIS data, J. Geophys. Res., 112, D09208, doi:10.1029/2006JD007778, 2007.

Closure on the single scattering albedo

J. C. Barnard et al.

Querol, X., Pey, J., Minguillón, M. C., Pérez, N., Alastuey, A., Viana, M., Moreno, T., Bernabé, R. M., Blanco, S., Cárdenas, B., Vega, E., Sosa, G., Escalona, S., Ruiz, H., and Artíñano, B.: PM speciation and sources in Mexico during the MILAGRO-2006 Campaign, Atmos. Chem. Phys., 8, 111–128, 2008,

5   http://www.atmos-chem-phys.net/8/111/2008/.

Quinn, P. K., Anderson, T. L., Bates, T. S., Dlugi, R., Heintzenberg, J., Hoyningen-Huene Von, W., Kulmala, M., Russell, P. B., and Swietlicki, E.: Closure in troposheric aerosol-climate research: a review and future needs for addressing aerosol direct shortwave radiative forcing, Contr. Atmos. Phys., 69, 547–577, 1996.

10   Quinn, P. K. and Coffman, D. J.: Local closure during the First Aerosol Characterization Experiment (ACE 1): Aerosol mass concentration and scattering and backscattering coefficients, J. Geophys. Res., 103(D13), 16575–16596, 1998.

Rahmah, A. A., Arnott, W. P., and Moosmüller, H.: Integrating nehelometer with a low truncation angle and an extended calibration scheme, Meas. Sci. Technol., 17, 1723–1732, 2006.

15   Ramanathan, V., Crutzen, P. J., Kiehl, J. T., and Rosenfeld, D.: Aerosols, climate, and the hydrological cycle, Science, 7, 2119–2124, 2001.

Russell, P. B. and Heintzenberg, J.: An overview of the ACE-2 clear sky column closure experiment (CLEARCOLUMN), Tellus B, 32, 463–483, 2000.

Schmid. B., Livingston, J. M., Russell, P. B., Durkee, P. A., Jonsson, H. H., Collins, D. R.,
20   Flagan, R. C., Seinfeld, J. H., Gassó, S., Hegg, D. A., Öström, E., Noone, K. J., Welton, E. J., Voss, K. J., Gordon, H. R., Formenti, P., and Andreae, M.: Clear-sky closure studies of lower tropospheric aerosol and water vapor during ACE-2 using airborne sunphotometer, airborne in-situ, space-borne, and ground-based measurements, Tellus B, 52, 568–593, 2000.

Sciare, J., Oikonomou, K., Cachier, H., Mihalopoulos, N., Andreae, M. O., Maenhaut, W., and
25   Sarda-Estéve, R.: Aerosol mass closure and reconstruction of the light scattering coefficient over the Eastern Mediterranean Sea during the MINOS campaign, Atmos. Chem. Phys., 5, 2253–2265, 2005,
      http://www.atmos-chem-phys.net/5/2253/2005/.

Shaw, W. J., Allwine, K. J., Fritz, B. G., Rutz, F. C., Rushel, J. P., and Chapman, E. G.: An
30   evaluation of the wind erosion module in DUSTRAN, Atmos. Environ., 42, 1907–1921, 2008.

Sokolik, I. N. and Toon, O. B.: Incorporation of mineralogical composition of aerosols into models of radiative properties of mineral aerosol from the UV to IR wavelengths, J. Geophys. Res., 104(D8), 9423–9444, 1999.

Closure on the single scattering albedo

J. C. Barnard et al.

Title Page

Abstract	Introduction
Conclusions	References
Tables	Figures

| ◄◄ | ►► |
| ◄ | ► |

| Back | Close |

Full Screen / Esc

Printer-friendly Version

Interactive Discussion

Subramanian, R., Roden, C. A., Boparai, P., and Bond, T. C.: Yellow beads and missing parti-
cles: Trouble ahead for filter-based absorption measurements, Aerosol Sci. Tech., 41, 630–
637, 2007.

Turpin, B. J. and Lim, H.-J.: Species contributions to $PM_{2.5}$ mass concentrations: revisiting
common assumptions for estimating organic mass, Aerosol Sci. Tech., 35, 602–610, 2001.

Wang, J., Flagan, R. C., Seinfeld, J. H., Jonsson, H. H., Collins, D. R., Russell, P. B., Schmid,
B., Redemann, J., Livingston, J. M., Goa, S., Hegg, D. A., Welton, E. J., and Bates, D.:
Clear-column radiative closure during ACE-Asia: Comparison of multi-wavelength extinction
derived from particle size and composition with results from Sun photometry, J. Geophys.
Res., 107(D23), 4688, doi:10.1029/2002JD002465, 2002.

Weber, R. J., Orsini, D., Daun, Y., Lee, Y.-N., Klotz, P. J., and Brechtel, F.: A particle-to-liquid
collector for rapid measurement of aerosol bulk chemical composition, Aerosol Sci. Tech.,
35, 718–727, 2001.

Zaveri, R. A., Easter, R. C., Fast, J. D., and Peters, L. K.: Model for simulating
aerosol interactions and chemisty (MOSAIC), J. Geophys. Res., 113(D13), D13204,
doi:10.1029/2007JD008782, 2008.

ACPD

9, 5009–5054, 2009

Closure on the single scattering albedo

J. C. Barnard et al.

Title Page

Abstract	Introduction
Conclusions	References
Tables	Figures

◄ ►

◄ ►

Back Close

Full Screen / Esc

Printer-friendly Version

Interactive Discussion

Table 1. Aerosol properties and associated measurements used in the closure experiment.

Aerosol property	Instrument/Comment
Elemental Carbon (EC)	Sunset Laboratories OCEC instrument (Birch and Cary, 1996)
Organic Carbon (OC)	Sunset Laboratories OCEC instrument (Birch and Cary, 1996)
Inorganic species (Na, Ca, Mg, NH_4, NO_3, etc.)	PILS (Weber et al., 2001)
Aerosol water	Not measured, but the aerosols are probably dry (Moffett et al., 2008a, b)
Dust	Inferred from PM_{10} and $PM_{2.5}$
Aerosol absorption (870 nm)	Photoacoustic spectrometer (Paredes-Miranda et al., 2008)
Aerosol scattering	Photoacoustic spectrometer; reciprocal nephelometry
Aerosol size distribution (fine mode) (Paredes-Miranda et al., 2008)	Inferred from AERONET, $PM_{2.5}$, and PM_{10} measurements
Aerosol size distribution (coarse mode)	Inferred from AERONET, $PM_{2.5}$, and PM_{10} measurements

Table 2. Refractive indices ($n+ik$) of the indicated species at 870 nm.

Species	Density (g/cm^3)	Refractive index (real), n	Refractive index (imaginary), k
SO$_4$	1.8	1.52	0
NO$_3$	1.8	1.5	0
NH$_4$	1.8	1.5	0
Cl	2.2	1.45	0
Na	2.2	1.45	0
Ca	2.6	1.56	0
Mg	1.8	1.5	0
Organic Matter (OM) (Kanakidou et al., 2005)	1.4	1.45	0
Elemental Carbon (EC) (Bond and Bergstrom, 2006)	1.8	1.85	0.71
Dust (Clarke et al., 2004; Prasad and Singh, 2007; Mishra and Tripathi, 2008)	2.6	1.55	0.004
Water	1.0	1.33	0.0

Table 3. Change in B_{scat}, B_{abs}, and ϖ_0 for a 10% change in the indicated variables in column 1. In this table, "n" stands for the real part of the refractive index, and "k" stands for the imaginary part. The far right-hand column in this table provides an estimated uncertainty for the variable listed in the first column. Density uncertainties, not listed here, are ±6% for BC, and are assumed to be ±10% for all other materials.

Variable	ΔB_{scat} (Mm^{-1})	ΔB_{abs} (Mm^{-1})	$\Delta \varpi_0$	Estimated uncertainty of the variable
BC mass concentration	−0.065	**1.74**	**−0.025**	0.2 μg/m^3
PM$_{2.5}$	**4.21**	0.41	0.017	±5%
Inorganic mass concentration	0.12	−0.085	0.0025	10% (Weber et al., 2001);
OM mass concentration	0.41	−0.094	0.0043	0.3 μg/m^3
n (BC)	2.4	−0.22	0.019	1.75 to 1.95 (Bond and Bergstrom, 2006), ±6%
k (BC)	−0.45	**1.65**	**−0.026**	0.64 to 0.79 (Bond and Bergstrom, 2006), ±10%
n (dust)	**6.87**	**0.61**	0.025	±5% (Clarke et al., 2004; Prasad and Singh, 2007)
k (dust)	−0.013	0.043	0.0	±100% (Clarke et al., 2004; Prasad and Singh, 2007; Mishra and Tripathi, 2008)
n (OM)	**9.5**	**0.93**	**0.044**	±5% (Kanakidou et al., 2005)
n (inorganic)	**6.7**	0.60	**0.030**	±5%

[ACPD](#)

9, 5009–5054, 2009

Closure on the single scattering albedo

J. C. Barnard et al.

Title Page

Abstract | Introduction

Conclusions | References

Tables | Figures

◀◀ | ▶▶

◀ | ▶

Back | Close

Full Screen / Esc

Printer-friendly Version

Interactive Discussion

**Closure on the single scattering albedo**

J. C. Barnard et al.

**Table 4.** Mean values of observed and calculated (modal model and CTOM) aerosol optical properties for the period 15 through 27 March 2006. The observations are shown with their systematic uncertainties. The calculations do not have uncertainties because adjustments have been made with estimated uncertainty ranges to achieve closure. The boldface type indicates a variable where closure is not achieved.

Optical property	Observations (with uncertainties)	Modal model	CTOM
ϖ_0	0.77±0.05	0.80	0.79
B_{scat}	33.3 Mm^{-1}±5.00 Mm^{-1}	34.1 Mm^{-1}	36.3 Mm^{-1}
B_{abs}	9.22 Mm^{-1} ± 0.92 Mm^{-1}	9.94 Mm^{-1}	**10.96** Mm^{-1}
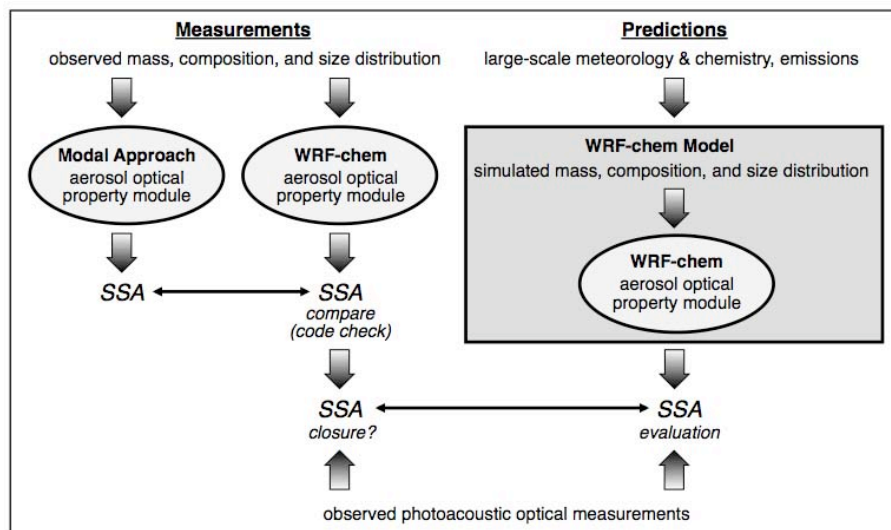
Fig. 1. Schematic of closure study (left hand side), and evaluation of the calculated aerosol optical properties from the full WRF-Chem model (right hand side).
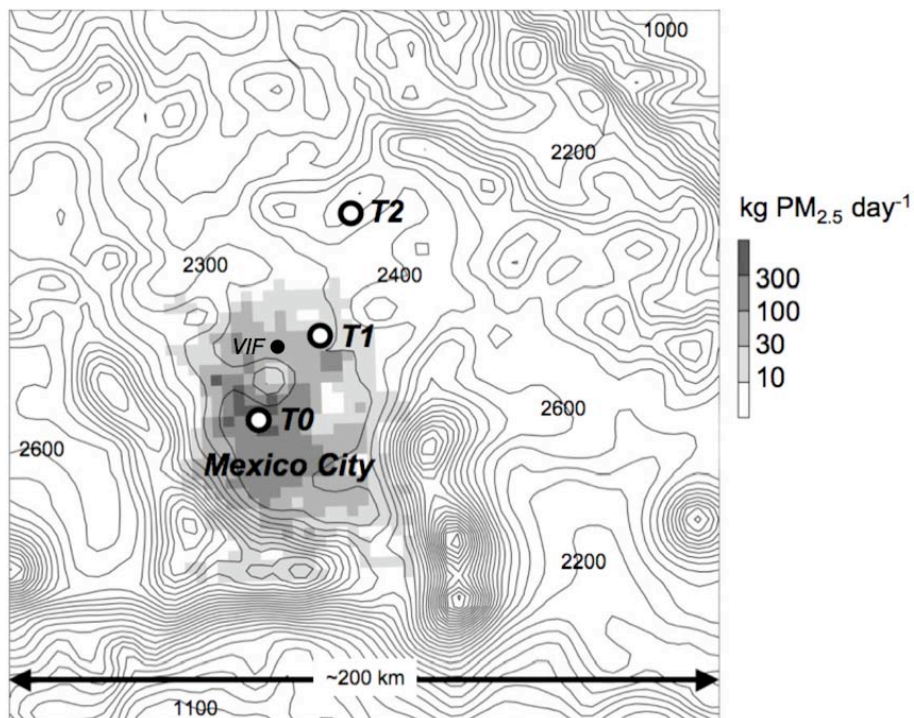
Fig. 2. Map of MCMA showing the VIF, T0, T1, and T2 sites. The shaded areas indicate the estimated $PM_{2.5}$ emissions, which roughly show the outline of MCMA.

ACPD

9, 5009–5054, 2009

Closure on the single scattering albedo

J. C. Barnard et al.

Title Page

Abstract | Introduction

Conclusions | References

Tables | Figures

◀ | ▶|

◀ | ▶

Back | Close

Full Screen / Esc

Printer-friendly Version

Interactive Discussion

Closure on the single scattering albedo

J. C. Barnard et al.
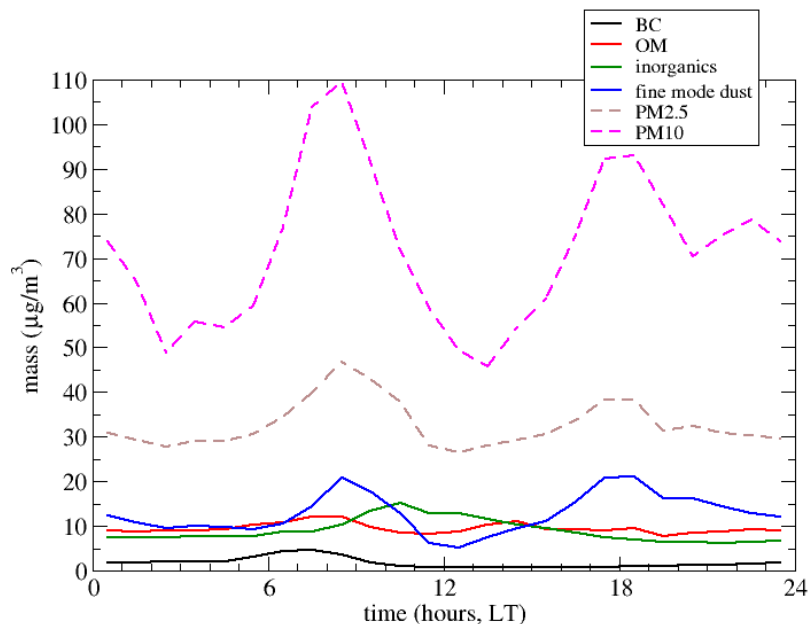
**Fig. 3.** Observed diurnal variation of aerosol chemical components, as well as PM$_{2.5}$ and PM$_{10}$ mass. The measurements over which the diurnal averages were taken extend from 15 through 27 March 2008.
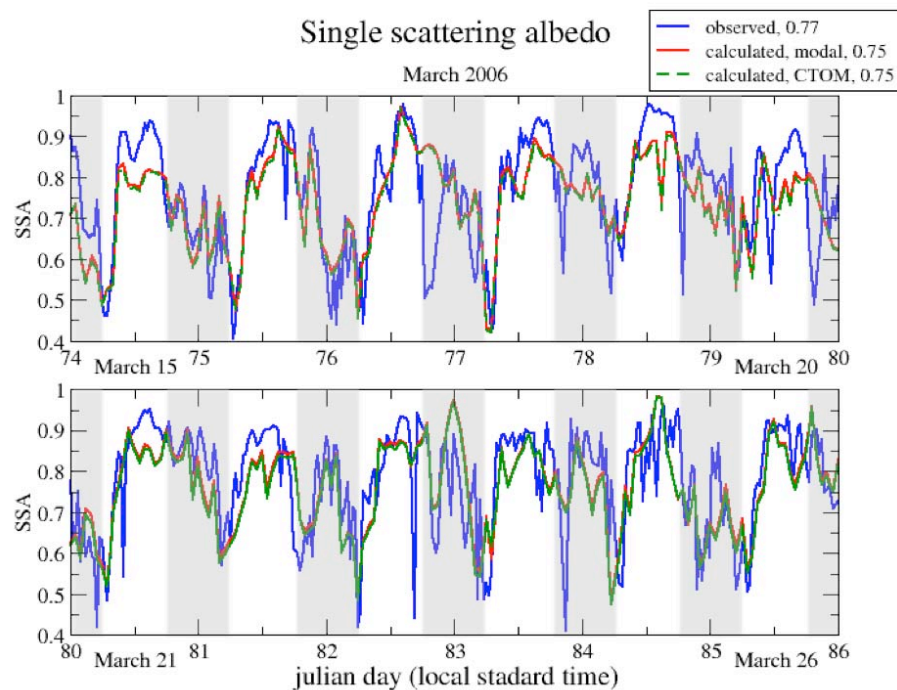
Fig. 4. Single scattering albedo, observed (blue) and calculated: modal (red), and CTOM (green). The averages of the three methods are given in the legend. The shaded areas indicate approximately the nighttime hours.

ACPD

9, 5009–5054, 2009

Closure on the single scattering albedo

J. C. Barnard et al.

Title Page

Abstract	Introduction
Conclusions	References
Tables	Figures

|◄ | ►|

◄ | ►

Back | Close

Full Screen / Esc

Printer-friendly Version

Interactive Discussion
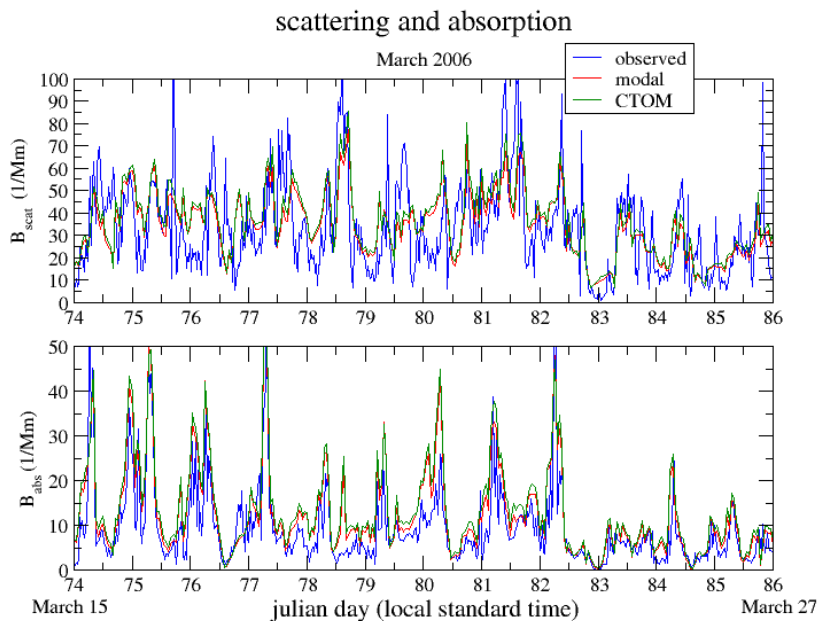
Fig. 5. Calculated and observed scattering (top panel) and absorption (bottom panel) coefficients, B_{abs} and B_{scat}, respectively. For the scattering coefficients, the model and CTOM results are about the same, but exceed the observations. This conclusion is generally true for the absorption, as well.
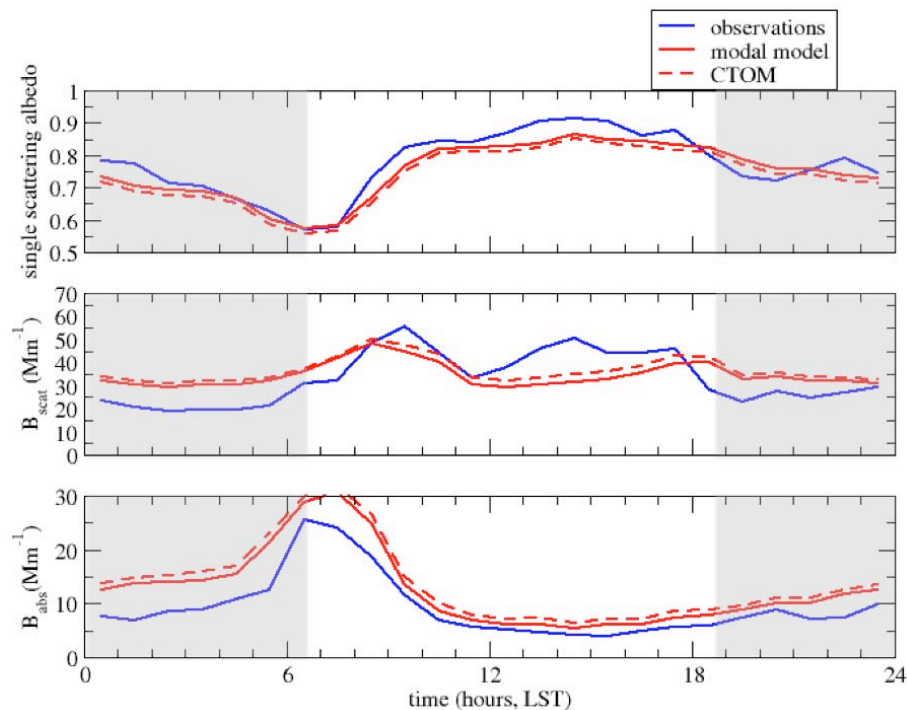
Fig. 6. The upper panel shows the diurnal variation of ϖ_0, averaged from day 74 (15 March 2006) to day 86 (27 March 2006). The two lower panels show the same for B_{abs} and B_{scat}. The shaded areas of the figure indicated the nighttime hours.
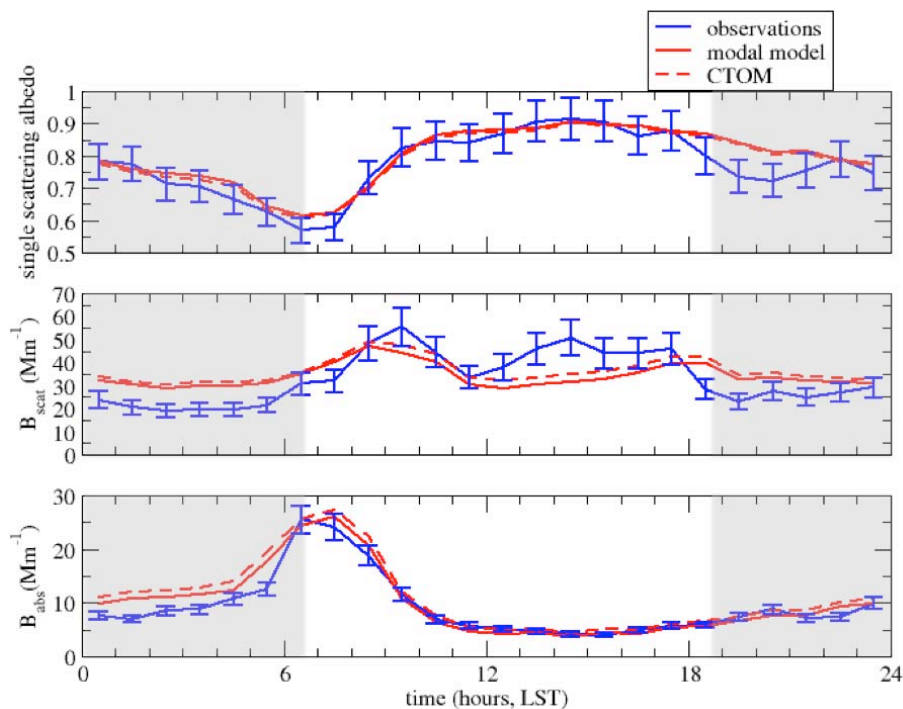
Fig. 7. Attempt at closure, based on hourly averages. The error bars represent uncertainties of 6%, 15%, and 10%, for ϖ_0, B_{scat}, and B_{abs}, respectively. The shaded areas of the figure indicate the nighttime hours.
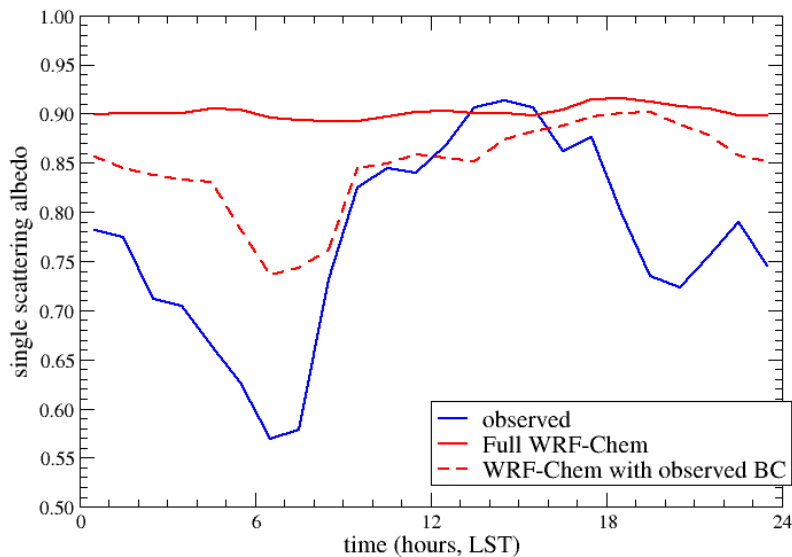
Fig. 8. Diurnal variation of ϖ_0 (similar to top panel Fig. 6). The observations are shown by the blue line. Simulations from the full, "online" WRF-Chem model are indicated by the red line. Simulations from the full WRF-Chem model, but with the predicted BC concentration replaced by the observed BC concentration, are indicated by the dashed red line.